Cross-regulation between CDK and MAPK control cellular fate

Eric Durandau, Serge Pelet*

Department of Fundamental Microbiology, University of Lausanne, CH-1015 Lausanne, Switzerland

* Corresponding author: serge.pelet@unil.ch

Keywords

MAPK signaling, cell cycle, yeast mating, single cell analysis, fluorescent biosensors

Abstract

Commitment to a new cell cycle is controlled by a number of cellular signals. Mitogen-Activated Protein Kinase pathways, which transduce multiple extracellular cues, have been shown to be interconnected with the cell cycle. Using budding yeast as a model system, we have quantified in hundreds of live single cells the interplay between the MAPK regulating the mating response and the Cyclin-Dependent Kinase controlling cell cycle progression. Different patterns of MAPK activity dynamics could be identified by clustering cells based on their CDK activity, denoting the tight relationship between these two cellular signals. In mating mixtures, we have verified that the interplay between CDK and MAPK activities allows cells to select their fate, preventing them from being blocked in an undesirable cellular program.

Introduction

Cells have developed complex signal transduction pathways to respond to changes in their environment. Plasma membrane sensors detect extracellular stimuli and relay this information inside the cell via signaling cascades. These protein networks can integrate multiple information to launch the appropriate cellular response. For instance, Mitogen-Activated Protein Kinase (MAPK) pathways are central nodes in the signaling network of eukaryotic cells, because they relay extracellular cues such as growth factors or stresses (Roux and Blenis, 2004; Chen and Thorner, 2007). The metabolic state, the cellular morphology or the cell cycle phase of individual cells can be integrated by the MAPK cascade to finely tune the cellular response (Strickfaden *et al.*, 2007; Nagiec and Dohlman, 2012; Clement *et al.*, 2013). However, the molecular mechanisms that allow these signal integrations are generally unknown.

The simplified settings offered by *S. cerevisiae* provide an ideal platform to study these complex mechanisms. The budding yeast MAPK network is composed of four main pathways active in haploid cells (Saito, 2010). Multiple instances of signal integration have been documented in this model system: the cross-inhibition between two MAPK pathways (Nagiec and Dohlman, 2012), the limitation of signal transmission in low nutrient conditions (Clement *et al.*, 2013; Sharifian *et al.*, 2015) and the tight coupling between cell cycle regulation and MAPK activity (Oehlen and Cross, 1994; Peter and Herskowitz, 1994; Wassmann and Ammerer, 1997; Escoté *et al.*, 2004; Clotet and Posas, 2007; Strickfaden *et al.*, 2007). In this study, we were interested in the interplay between the cell cycle and the mating pathway.

Haploid budding yeasts exist in two mating types: *MAT***a** and *MAT*$\boldsymbol{\alpha}$. They produce pheromones (respectively a-factor and α-factor) that can be sensed by a mating partner. Activation of a G-protein-coupled receptor by the pheromone leads to the activation of the MAPKs Fus3 and Kss1, via a three-tier kinase cascade recruited to the plasma membrane by the scaffold protein Ste5 (Bardwell, 2005; Atay and Skotheim, 2017). The two MAPKs initiate a mating program that includes the transcription of hundreds of genes, the arrest of the cell cycle in G1, the formation of a mating projection and which culminates in the fusion of the two partners.

In order to guarantee that each cell that undergoes fusion possesses a single copy of its genome, active Fus3 phosphorylates the Cyclin Kinase Inhibitor (CKI) Far1 which arrests the cells in G1 (Peter *et al.*, 1993; Peter and Herskowitz, 1994). In addition, during division, signaling in the

31 mating pathway is dampened by the action of the Cyclin Dependent Kinase (CDK) Cdc28.
32 Cdc28, the only CDK in *S. cerevisiae*, associates with the different cyclins to ensure the proper
33 progression through the cell cycle. Inhibition of the mating pathway is made possible by the
34 association between the CDK and the late-G1 cyclins Cln1 and Cln2. The Cln1/2-Cdc28
35 complex has been shown to phosphorylate the scaffold protein Ste5, thereby preventing its
36 recruitment to the plasma membrane and thereby preventing the transduction of the signal from
37 the receptor to the MAPK cascade (Strickfaden *et al.*, 2007).

38 Most of the knowledge on the mating-induced cell cycle arrest in G1 and the inhibition of the
39 mating pathway during division has been obtained from population-level measurements, relying
40 on artificial synchronizations of the cell cycle using temperature sensitive mutants, chemical
41 inhibitors or by overexpression of cyclins (McKinney *et al.*, 1993; Peter *et al.*, 1993; Wassmann
42 and Ammerer, 1997; Strickfaden *et al.*, 2007). More recent studies have used single cell
43 measurements to monitor this cross-inhibition, but focused either on Ste5 relocation (Repetto *et*
44 *al.*, 2018) MAPK activity (Durandau *et al.*, 2015; Conlon *et al.*, 2016) or on CDK activity
45 (Doncic *et al.*, 2015).

46 In this study, we have developed a sensitive assay enabling to quantify in parallel MAPK and
47 CDK activity in non-synchronized live single cells using fluorescent biosensors. By exploiting
48 the natural diversity present in the population, we have been able to cluster cells based on their
49 cell cycle position and monitored their MAPK activity pattern. We could confirm the key role of
50 Far1 for the G1 arrest. However, our data suggest that an additional mechanism working in
51 parallel with the Ste5 phosphorylation is required to limit signaling during S-phase. Furthermore,
52 we highlight the importance of the cross-inhibition between MAPK and CDK for cell-fate
53 decision in the mating process. The interplay between these two activities will determine whether
54 cells induce a mating response or commit to a new cell cycle round.

55 Results

56 *Quantifying MAPK activity*

57 In order to quantify mating MAPK activity, we have developed a Synthetic Kinase Activity
58 Relocation Sensor (SKARS). This probe was engineered by combining a specific MAPK
59 docking site, a phosphorylatable Nuclear Localization Signal (NLS) and a Fluorescent Protein

60 (FP) (Durandau *et al.*, 2015). The docking site consists in the first 33 amino acids from the
61 MAP2K Ste7, which confers specificity towards both Fus3 and Kss1 (Reményi *et al.*, 2005).
62 Under normal growth conditions, the NLS promotes the enrichment of the sensor in the nucleus.
63 Upon activation of the MAPK, specific residues neighboring the NLS are phosphorylated by the
64 targeted MAPK, leading to a decrease in the import rate of the sensor in the nucleus. The
65 presence of the FP allows monitoring nuclear-to-cytoplasmic partitioning of the sensor as
66 function of time (Figure 1A). We use two bright field images and a fluorescence image of the
67 nucleus (Hta2-tdiRFP) to segment the nuclear and cytoplasmic areas in each cell and measure the
68 fluorescence intensity in the other fluorescent images acquired (Pelet *et al.*, 2012). The ratio of
69 mean fluorescence intensities between these two compartments in the RFP channel provides a
70 dynamic measure of MAPK signaling activity in each single cell.

71 One experimental difficulty associated with this sensing strategy is the fact that each cell has a
72 distinct inherent capacity to import the sensor in the nucleus. Therefore, the read-out provided
73 for each cell includes an additional undesired component. In order to correct for this
74 experimental variability, we introduced, in parallel to the functional sensor present in the RFP
75 channel, a non-functional sensor in the CFP channel based on a version of the reporter that
76 cannot bind the kinase (non-docking sensor, $Ste7_{ND}$-SKARS, Figure 1B). We define the MAPK
77 activity as the ratio of cytoplasmic-to-nuclear fluorescence of the functional sensor over the ratio
78 of cytoplasmic-to-nuclear fluorescence of the non-docking corrector (Supplementary Figure 1
79 and Methods). This metric provides a relative measure of the combined Fus3 and Kss1 activity
80 independently of the nuclear import capacity of each cell.

81 We have performed time-lapse experiments where cells are stimulated with synthetic pheromone
82 at saturating concentration (1000nM α-factor) directly under the microscope. The dynamics of
83 activation of the mating pathway in single cells can be quantified (Figure 1C). In comparison
84 with a signaling dead mutant (*ste5*Δ), we observe a clear increase in the median MAPK activity
85 of the population within 5 minutes after the stimulus. However, the few single cell traces plotted
86 in this figure display strikingly different dynamic behaviors, demonstrating well the great
87 heterogeneity in the signaling capacity of individual cells.

88 *Monitoring CDK activity*

89 Because it has been established for a long time that the cell cycle can influence mating signaling
90 competence, we decided to monitor in the same cells both MAPK and CDK activities to
91 overcome the need for population average measurement and artificial cell cycle synchronization.
92 In order to follow cell cycle progression in an automated and robust manner, we used a
93 fluorescently tagged Whi5, which has been used in many studies as an endogenous relocation
94 probe for the G1 state (Bean *et al.*, 2006; Doncic *et al.*, 2011). Whi5 is enriched in the nucleus of
95 the cells in G1 to repress the expression of specific cell cycle genes. Phosphorylation by the
96 Cln3-CDK complex relieves this repression by promoting the nuclear export of Whi5 (Costanzo
97 *et al.*, 2004; de Bruin *et al.*, 2004) (Figure 1D and E). Whi5 will only shuttle back into the
98 nucleus as cells re-enter in G1. Thus, in addition to the SKARS and its corrector, we tagged
99 Whi5 with mCitrine and measured the cytoplasmic to nuclear fluorescence intensity in the YFP
100 channel as a proxy for CDK activity (Figure 1F). Note that during the division process,
101 fluctuation in CDK activity levels cannot be quantified using this approach, but the Whi5 probe
102 allows us to precisely monitor the exit from G1 and the entry into G1. In the dataset of a two-
103 hour time-lapse movie, we collected single cell traces that displayed a transient nuclear
104 accumulation of Whi5. The rapid accumulation of Whi5 in the nucleus, which corresponds to the
105 sharp decrease in CDK activity occurring at the onset of G1, was used to synchronize
106 computationally the single cell traces (Figure 1F and Supplementary Figure 2). The alignment of
107 the single-cell responses reveals two additional CDK activity drops taking place roughly 90
108 minutes before or after the central trough. This timing matches the expected cell cycle length in
109 these conditions (Charvin *et al.*, 2008). To sum up, this reporter strain allows us to monitor in
110 parallel CDK and mating MAPK activities in single cells, thereby providing an assay to
111 disentangle their interactions.

112 *Cell cycle stage clustering*

113 In a naturally cycling population of budding yeast cells, all cell cycle stages are represented at a
114 given time point. Therefore, when this population is stimulated with α-factor, in a single
115 experiment, we can observe the entire diversity of responses present in the population generated
116 by this extrinsic variability. In a typical time-lapse experiment of 45 minutes, cells are imaged
117 every 3 min and the pheromone is added before the third time point. From such a microscopy
118 dataset, several hundreds of single cells are tracked and pass through a quality control filter. Note
119 that unless stated otherwise, all following experiments with exogenous pheromone stimulation

120 are performed in a *bar1*Δ background, to maintain a constant extracellular concentration of α-
121 factor in the medium surrounding the cells and were performed in at least three independent
122 experiments.

123 The single cell traces are clustered *in silico* based on their CDK activity pattern to identify the
124 different cell-cycle stage populations (see Methods). The first cluster consists of cells with low
125 CDK activity throughout the time lapse (*G1*, 20% of the population). These *G1* cells are MAPK
126 signaling competent and display a strong and sustained response of the SKARS upon addition of
127 pheromone (Figure 2A). A second cluster is made of cells with a high CDK activity during the
128 45 minutes of the time lapse (*Out-of-G1*, 35%). These cells display a fast response to the mating
129 pheromone but with a low amplitude. Previous reports have shown, by overexpression of cyclins,
130 that the activity of the CDK can abolish or strongly reduce the activity of the mating pathway
131 (Oehlen and Cross, 1994; Wassmann and Ammerer, 1997). Under physiological conditions, our
132 data show that dividing cells are none-the-less able to activate the MAPK pathway, but only
133 weakly compared to the *G1* cells.

134 In addition, our dynamic measurements can reveal interesting signaling patterns by focusing our
135 analysis on cells that transition between these two strong and weak signaling states (*G1* and *Out-*
136 *of-G1*, respectively). A third cluster was thus defined with cells that start with a low CDK
137 activity and end with high CDK activity. These cells are thus exiting G1 and enter S-phase at
138 some point during the time lapse (*G1-exit* 11%, Figure 2C). Interestingly, these cells respond
139 strongly to the pheromone stimulus, but display a transient MAPK activation behavior. When
140 pheromone is added, the mating pathway is first rapidly activated. However, when the CDK
141 activity builds up in the cell, an inhibition of the MAPK pathway sets in, leading to a return of
142 the MAPK activity to a low level roughly 15 min after the stimulus.

143 The fourth cluster consists in cells that enter in G1 during the time lapse (*G1-entry*, 31%). These
144 cells start with high CDK activity and end the time lapse with low CDK activity. This transition
145 can happen at any time point during the experiment. The median MAPK activity in this sub-
146 population increases gradually with time, while the individual traces display sharp transitions
147 from a low signaling to a high-signaling state (Supplementary Figure 3A). Using the Whi5
148 reporter, the single cell traces were temporally aligned based on the time of G1 entry. As a result,
149 a synchronous increase in MAPK activity is observed when CDK activity stabilizes to low
150 values, corresponding to the G1-phase (Figure 2D and Supplementary Figure 3B). Finally, a fifth

151 cluster was identified with cells that cycle briefly in G1 during the time lapse (*Through-G1*, 3%).
152 No specific behavior in MAPK activity was observed in these cells even when traces are aligned
153 relative to the time of G1 entry (Supplementary Figure 4).

154 Figure 2E allows a direct comparison of the MAPK activity measured with the SKARS in
155 different cell cycle stages. The mean response of the population (thick blue line) is not
156 representative of the behavior of individual cells which can display strikingly different behavior.
157 However, because CDK plays a major role in controlling the signaling output of the mating
158 pathway, clustering based on the CDK activity pattern allows to group together cells that display
159 similar MAPK activity dynamics. Thus, we observe four types of behaviors: strong and sustained
160 activity for *G1* cells, weak and sustained activity in *Out-of-G1* cells, strong but transient activity
161 in the *G1-exit* cluster and delayed activation (depending on the timing of CDK activity drop)
162 present in the *G1-entry* cells.

163 *Comparison with other reporters*

164 In order to compare the results obtained with the SKARS, we performed a similar analysis with
165 two different assays that report on mating pathway activity. Using a fluorescently tagged Kss1
166 (Kss1-mScarlett), the relocation of the MAPK from the nucleus to the cytoplasm upon
167 pheromone stimulus has been monitored in a strain carrying Whi5-mCitrine. This change in
168 cellular compartments of Kss1 has been shown to be a consequence of the disassembly of a
169 complex formed between Dig1/Dig2, Ste12 and Kss1, upon phosphorylation by Fus3 and/or
170 Kss1 (Pelet, 2017) (Supplementary Figure 5 A and B). When comparing the response of the cells
171 in different cell-cycle stages, a similar pattern can be observed between this assay and the
172 SKARS reporter (Supplementary Figure 6). The major difference can be observed in the *G1-*
173 *entry* cluster where a gradual increase in signaling activity can be seen upon entry into G1
174 (Supplementary Figure 6D), compared to the sharper dynamics of the SKARS reporter in the
175 same cell cycle stage (Figure 2D). In addition, when comparing the Kss1 relocation of *G1* and
176 *G1-entry* cells relative to the time of pheromone addition (Supplementary Figure 6E), we see that
177 they are almost identical. This suggests that cells late in the division process have fully recovered
178 their signaling ability.

179 The second assay is based on the dPSTR (dynamic Protein Synthesis Translocation Reporter)
180 system which allows to monitor the dynamics of induction of a promoter of interest (Aymoz *et*

181 *al.*, 2016). This promoter drives the expression of a small peptide that promotes the relocation of
182 a fluorescent protein in the nucleus of the cell. We use the previously published p*AGA1*-dPSTR
183 to monitor the dynamics of mating gene induction. AGA1 has been shown to be strongly induced
184 by α-factor in a MAPK dependent manner (Roy *et al.*, 1991; Oehlen *et al.*, 1996; Aymoz *et al.*,
185 2018). Clustering of the gene expression data based on cell-cycle stage demonstrates a strong
186 expression in *G1* and *G1-entry* clusters, while clusters for *Out-of-G1* and *G1-exit* cells display an
187 attenuated and delayed response (Supplementary Figure 7).

188 The global outcome that can be obtained by comparing these three types of reporters is that full
189 signal competence is observed in the *G1* cluster, while *Out-of-G1* cells have a reduced ability to
190 signal. In addition, cells exiting G1 will only transiently activate the MAPK. Interestingly, this
191 transient activation is not sufficient to drive gene expression as protein production in the *G1-exit*
192 cluster is delayed by 20 to 30 minutes.

193 *MAPK activity in the G1-entry cluster*

194 The comparison between the SKARS, the Kss1 relocation and the pAGA1-dPSTR also
195 highlights a discrepancy for the *G1-entry* cluster. While the two latter assays display a signaling
196 ability that is comparable to the one present in *G1* cells for the *G1-entry* cluster, the SKARS
197 measurements suggest that the MAPK activity is only recovered when CDK activity has
198 dropped, as cells enter in G1.

199 The influence of the cell cycle on the nuclear enrichment of the SKARS could potentially
200 explain this observation. Indeed, a lower enrichment of the corrector can be observed in *Out-of-*
201 *G1* cells compared to *G1* cells (Supplementary Figure 8A and B). In the *G1-entry* cluster, this
202 results in a slow transition from a low to a high nuclear to cytoplasmic ratio (N/C) of the
203 corrector around the time of entry into G1. In signaling dead cells, the exact same behavior is
204 observed for the functional sensor (Supplementary Figure 1B). However, the dynamic of this
205 transition is strikingly different from the dynamic of MAPK activity measured upon *G1-entry*.
206 While the corrector slowly rises from -10 to +10 min, the MAPK activity shift takes place
207 between +5 and +10 min after the CDK activity drop. Thus, the fact that these two events are not
208 synchronous, strongly suggests that the sharp increase in MAPK activity is not an artifact from a
209 reduced sensitivity during the division of the cells.

210 Because, in each individual cell, the sensor and corrector nuclear enrichment are highly
211 correlated (Supplementary Figure 8C), we performed an additional verification and separately
212 analyzed cells with low and high nuclear enrichment of the corrector (Supplementary Figure 8D
213 and E). If the G1-entry behavior was an artifact due to a poor enrichment of the sensor, we would
214 expect that cells with a relatively high nuclear enrichment would not display this behavior or at
215 least to a lower extent. On the contrary, we observe that *G1-entry* cells which keep a high N/C of
216 the corrector throughout the time-lapse display a stronger change in MAPK activity 10 minutes
217 after G1 entry.

218 In agreement with the Kss1 and dPSTR assays, previous works (Oehlen and Cross, 1994;
219 Wassmann and Ammerer, 1997; Strickfaden *et al.*, 2007; Conlon *et al.*, 2016), have shown that
220 CDK inhibition of the mating pathway is limited to the S-phase and full signaling competence is
221 recovered in G2-M. The dynamics observed with the SKARS are therefore unexpected. This
222 behavior could be explained by the action of phosphatases acting on the phosphorylated residues
223 present on the SKARS. For instance, the Cdc14 phosphatase leaves the nucleus during mitotic
224 exit to dephosphorylate cyclin-dependent targets (Shou *et al.*, 1999; Visintin *et al.*, 1999; Mohl *et*
225 *al.*, 2009). If this hypothesis is true, we can envision that other substrates of the MAPK might be
226 the target of phosphatases upon G1-entry and restrict their activity to the G1 phase.

227 *Pheromone dose response*

228 In order to test how the MAPK signaling behavior changes as function of input strength, time-
229 lapse movies were recorded with various concentrations of pheromone. The same cell cycle
230 clustering approach was used for all the dataset. As expected, the amplitude of the MAPK
231 activity decreases with lower pheromone concentrations (Figure 3 A-C). However, other changes
232 can also be observed between the different concentrations. In the G1-phase, a sustained MAPK
233 activity is observed at high doses of pheromone, while the signaling activity declines at lower α-
234 factor doses (Figure 3A). This behavior suggests an interplay between positive and negative
235 feedback loops. Multiple regulatory mechanisms have been identified in the mating pathway
236 (Hao *et al.*, 2003; Bhattacharyya *et al.*, 2006; Yu *et al.*, 2008; Nagiec *et al.*, 2015). None-the-
237 less, it remains difficult to estimate their relative influence on the signaling outcome. Our data
238 suggest that at low α-factor concentrations, negative feedbacks are prevalent and contribute to
239 the deactivation of the pathway. At high pheromone concentrations, however, the positive

240 feedbacks stabilize the system in a high activity state for a long time. Similar experiments were
241 performed in *BAR1*+ cells, where the presence of the pheromone protease adds another layer of
242 regulation to the system and leads to a faster decline in signaling activity at all concentrations but
243 the highest one, which remains sustained over the course of the time lapse experiment
244 (Supplementary Figure 9).

245 It is well-established that treatment with pheromone prevents cells from entering a new cell cycle
246 round (Hartwell *et al.*, 1974), therefore one expects a difference in the proportion of G1 cells at
247 the end of the experiment between α-factor treated and mock treated cells (Figure 3D).
248 Interestingly, we noticed a gradual increase in the fraction of cells retained in G1 as function of
249 pheromone concentration. If we focus on the population of cells starting in G1 (*G1* and *G1-exit*
250 clusters, which roughly represent one third of the population), in the untreated situation 20% will
251 exit G1, while 9% remain in G1 for the entire time lapse. Note that these measured percentages
252 are specific to our 45 min the time lapse. For the sample stimulated with pheromone, this
253 proportion gradually increases to reach 20% of cells that remain in G1 at 1000nM versus 10%
254 that can still escape G1 arrest. A similar behavior is observed for cells that are dividing at the
255 onset of the time lapse (*Out-of-G1* and *G1-entry*). The proportion of the cells that enter and stay
256 in G1 (*G1-entry*) evolves from 12% to 30% as pheromone concentration increases. Thus, the
257 stronger MAPK activity measured at high concentrations promotes a larger accumulation of cells
258 in G1 at the end of the time-lapse movie. These experiments clearly illustrate the fact that the
259 level of MAPK activity influences the ability of the cells to initiate division.

260 *START as a signal integration point*

261 The START event in the cell cycle has been operationally defined as the time when cells become
262 insensitive to a pheromone stimulus and are committed to a new cell cycle round (Hartwell *et al.*,
263 1974). Multiple cellular events are coordinated around this decision point. Activity of the G1
264 cyclin Cln3 increases. It triggers the exit of Whi5 out of the nucleus, thereby allowing the
265 transcription of Cln1 and Cln2. These two cyclins will in turn drive the transcription of
266 downstream S-phase genes (Dirick *et al.*, 1995; Costanzo *et al.*, 2004; de Bruin *et al.*, 2004). We
267 have shown that the number of cells that are blocked in G1 or commit to a new cell cycle round
268 is dependent on the pheromone concentration and thus on the MAPK activity. In parallel, we
269 observed that the CDK activity, estimated from the Whi5 nuclear enrichment levels, gradually

270 increases for cells that commit to a new cell cycle round (*G1-exit* cluster, Figure 4 A-D). At low
271 pheromone concentration, cells can often override the mating signal and enter the cell cycle.
272 However, at high concentrations of α-factor only cells that have already reached a sufficient
273 CDK activity will be able to counterbalance the mating signal. In these cells, the CDK promotes
274 the entry in a new division round. Interestingly, at saturating α-factor concentrations, some cells
275 display a transient activation of the CDK, suggesting that the addition of the pheromone
276 inhibited the progression of the cell cycle (Figure 4E). A behavior that has been previously
277 characterized by Doncic et al. (Doncic *et al.*, 2011). Taken together these results comfort the idea
278 that START is a signal integration point where the cells balance the relative MAPK and CDK
279 activities to determine their fate: division or mating.

280 Hence, the cross-inhibition between the MAPK and CDK plays a central role in the decision to
281 mate or divide. The molecular mechanisms regulating the interplay between mating and cell
282 cycle have been extensively studied. Phosphorylation and expression of Far1 upon α-factor
283 stimulus inhibit the Cln1/2-Cdc28 complex to prevent cell cycle progression into S-phase (Chang
284 and Herskowitz, 1990; Tyers and Futcher, 1993; Peter and Herskowitz, 1994). Deletion of FAR1
285 does not affect the MAPK signaling activity of *G1* nor of *Out-of-G1* cells (Supplementary Figure
286 10A). However, the fraction of cells found in G1 at the end of the time-lapse experiment is
287 increasing from 25% to 50% for WT cells when changing the pheromone concentration to 1μM,
288 while it remains below 30% in *far1*Δ (Supplementary Figure 10B). These results confirm the
289 important role played by Far1 in the G1-arrest during the mating response.

290 *Modulating Cdc28 activity*

291 We have shown above that the efficiency of the cell cycle arrest depends on the level of MAPK
292 activity. We next want to verify how the CDK activity influence the MAPK signal transduction.
293 In budding yeast, a single Cyclin Dependent Kinase, Cdc28, associates with the different cyclins
294 throughout the cell cycle to orchestrate the division of the cell. While Cdc28 is an essential
295 protein, it is none-the-less possible to acutely inhibit its kinase activity by using an analog
296 sensitive allele (*cdc28-as* (Bishop *et al.*, 2000)). The inhibitor NAPP1 was added to the cells 6
297 minutes after the pheromone stimulus. Upon NAPP1 treatment, *Out-of-G1* cells show a rapid
298 relocation of Whi5 in the nucleus, attesting the fact that CDK activity is blocked. In parallel, the

299 MAPK activity, that is low during division, increases to a level comparable to the one observed
300 in cells stimulated in G1 (Figure 5A).

301 Additionally, this experiment allows to verify that the transient MAPK activation observed in the
302 *G1-exit* cluster is shaped by the rising CDK activity. Cells with an increasing CDK activity after
303 pheromone stimulus were clustered. In the DMSO control experiment, this sub-population
304 displays the expected fast activation of the MAPK upon α-factor addition followed by a decay to
305 basal activity as CDK activity rises. In the inhibitor treated cells, the MAPK activity decay is
306 blocked upon NAPP1 addition and the MAPK signal rises to reach full activity (Figure 5B).
307 These experiments demonstrate that the activity of Cdc28 directly and quickly regulates the level
308 of MAPK activity present in the cell.

309 *Ste5 inhibition by the CDK*

310 One mechanism of inhibition of the mating pathway by the CDK has been shown to consist in
311 the direct phosphorylation of the scaffold Ste5 by the Cln1/2-Cdc28 complex (Strickfaden *et al.*,
312 2007). Eight consensus phosphorylation sites in the vicinity of a plasma membrane binding
313 domain (PM) in Ste5 are targeted by the CDK to alter the charge of this peptide. This
314 phosphorylation prevents the association of Ste5 to the membrane, thereby blocking the signal
315 flow in the pathway. In *ste5*Δ cells, we reintroduced three different alleles of Ste5 at the
316 endogenous locus: the WT copy, the $Ste5_{8A}$ mutant (where all putative phosphorylatable residues
317 were mutated to alanine (Strickfaden *et al.*, 2007)) or a $Ste5_{CND}$ (where the docking motif of
318 Cln1/2 on Ste5 has been mutated (Bhaduri and Pryciak, 2011)) (Figure 6A). We monitored the
319 response of the mating pathway for these three alleles with the SKARS, the relocation of Kss1
320 and the p*AGA1*-dPSTR at 10 and 100 nM α-factor (Figure 6B, C and D). The wild-type *STE5*
321 behaved similarly to the WT parental strains, demonstrating the functionality of the
322 complementation. As expected, signaling activity in *G1* cells is minimally influenced by either
323 mutation in Ste5 because the CDK is inactive. In the *G1-exit* cluster, the inhibition following the
324 transient activation of the pathway is less pronounced in the two Ste5 mutants than for the wild-
325 type allele. Generally, the behavior is more pronounced at 10nM than at 100nM α-factor and the
326 $Ste5_{8A}$ mutant displays a weaker inhibition by the CDK than the $Ste5_{CND}$ mutant.

327 A recent report has demonstrated that the combined action of Fus3 and Cdc28 is required to
328 phosphorylate the eight residues Ste5 in the vicinity of the PM domain (Repetto *et al.*, 2018).

329 However, our data suggest that an additional mechanism might contribute to limit the signal
330 transduction of the mating pathway in the early stage of the division process. This phenomenon
331 is best observed at low concentrations of pheromone where the activity of the MAPK cascade is
332 weaker. This behavior has not been detected previously, probably because most experiments
333 have been performed at saturating levels of pheromone. However, in mating mixture where
334 pheromone concentration is low, this mechanism could contribute to the cell fate decision. In
335 order to identify other potential targets of the CDK, we have tested various alleles of Ste20
336 because it has often been suggested as a potential target for this regulation (Oehlen and Cross,
337 1998; Wu *et al.*, 1998; Oda *et al.*, 1999) (Supplementary Figure 11A and C) and we have also
338 tested the influence of phosphorylation sites on Ste7 without measuring any detectable changes
339 in signaling activity between mutants (Supplementary Figure 11B and D).

340 To summarize, START is the integration point where MAPK and CDK activities are compared
341 to engage in a specific cellular fate. Far1 and Cdc28 are key players in this cross-inhibition of the
342 two pathways. *far1*Δ cells cannot arrest their cell cycle at START. None-the less, a number of
343 Far1-independent mechanisms for cell cycle arrest have been documented (Tyers, 1996; Oehlen
344 *et al.*, 1998; Cherkasova *et al.*, 1999). Cdc28 is solely responsible for the inhibition of the mating
345 pathway by the cell cycle and, up to now, only a single target, Ste5, has been convincingly
346 shown to regulate this process. Our data indicate that other mechanisms, that remain to be
347 identified, contribute to the repression of MAPK activity in dividing cells.

348 *MAPK activity in mating*

349 After studying the response of cells stimulated by exogenous pheromone, we next wanted to
350 understand how the cell cycle and the mating pathway were regulated during mating and how
351 this cross-inhibition allowed an efficient cell-fate selection in these physiological conditions. In
352 order to achieve this, we have imaged the *MAT***a** cells bearing the SKARS, the corrector and the
353 Whi5 marker in presence of a *MAT*α partner expressing constitutively a cytosolic CFP at high
354 levels. In Figure 7A, thumbnails of such an experiment are displayed. The fusion events (arrow
355 heads) can be detected by observing a sudden increase in CFP signal in the *MAT***a** cells. In the
356 frame preceding the two fusion events displayed in Figure 7A, we observe that the *MAT***a** cells of
357 interest are in G1 (nuclear Whi5) and display a high MAPK activity (nuclear depletion of the
358 SKARS).

359 The dynamic measurements of the mating process allowed us to monitor how cells reach this
360 state. Using our automated image analysis pipeline, we have detected more than one hundred
361 fusion events and curated them manually to remove any artifacts due to a mis-segmentation of
362 the cells. The single cell traces of these events have been computationally aligned relative to the
363 fusion time. Time zero corresponds to the last frame before the increase in CFP intensity,
364 because it is the last time point where MAPK activity can be reliably quantified (Figure 7B). As
365 a reference, the median MAPK activity of cells imaged under the same conditions but in absence
366 of a mating partner is plotted. In the fusing cell, a gradual increase in MAPK activity starts 40 to
367 60 minutes prior to fusion. In parallel, we observe that the median CDK activity is low for all
368 time-points. However, the 75 percentile stabilizes to a low value 40 minutes prior to fusion,
369 denoting that a fraction of the population enters in G1 within the hour preceding the fusion.

370 From the analysis of these fusion events, it becomes clear that the enrichment in G1 state prior to
371 fusion occurs in cells that experience a low level of MAPK activity, or, in other words, when
372 cells are surrounded by a low concentration of mating pheromone. In the exogenous stimulation
373 experiments, we have shown that at low pheromone concentrations, a fraction of the cells do not
374 commit to the mating response and keep proliferating. We verified if in the mating mixtures non-
375 fusing cells were influenced by the presence of the mating partners. To achieve this, we
376 monitored the CDK activity in cells that were cycling through G1. Interestingly, we observe that
377 the G1 state of these cells is prolonged and displays a great variability (Figure 7C). In these
378 cycling cells, the CDK activity remains lower in cells in mating mixtures compared to the same
379 cells imaged alone (Figure 7D). In parallel, a weak activation of the mating pathway can be
380 observed during the G1 phase (Figure 7E). *ste5*Δ cells imaged in presence of a mating partner
381 display a fast cycling through G1 compared to the WT cells because they remain insensitive to
382 the presence of the partners. In this background, the deletion of the scaffold Ste5 leads to an
383 absence of activity of the MAPK Fus3 and Kss1 which cannot counteract the rise of the CDK
384 activity at START.

385 **Discussion**

386 In this study, we performed dynamic single cell measurements with live-cell imaging. These
387 time lapse movies were automatically quantified, allowing the clustering and *in silico*
388 synchronization of hundreds of single cell traces. The ability to follow the response of individual

389 cells in a population of naturally cycling cells has enabled us to monitor the influence of the cell
390 cycle on the mating process with minimal perturbations. Importantly, the correlation of multiple
391 signaling activities within the same cell by combining fluorescent reporters for CDK and MAPK
392 activities allowed us to identify different MAPK signaling patterns, which demonstrates the
393 ability of the MAPK cascade to integrate the CDK activity to deliver the required signaling
394 output. The molecular mechanisms of some of these integrations have been identified previously,
395 but our quantitative measurements suggest that additional mechanisms contribute to the interplay
396 between MAPK and CDK.

397 We have verified with exogenous stimulation experiments performed with various
398 concentrations of pheromone that START is a central integration point where cells compare the
399 relative levels of MAPK and CDK activities to decide on their cellular fate: proliferation or
400 mating. It remains to be precisely determined which molecular mechanisms control this decision.
401 On the MAPK side, our data agree with the numerous previous studies that demonstrated that the
402 MAPK activity controls the CDK via the protein Far1 (Peter *et al.*, 1993; Peter and Herskowitz,
403 1994). The mating pathway regulates both the level of Far1 and its phosphorylation status. What
404 remains to be understood is how each one of these changes influence the decision made by the
405 cell.

406 On the CDK side, Cdc28 kinase activity is directly regulating the signal flow in the MAPK
407 pathway. Blocking Cdc28 activity relieves this inhibition allowing recovering full MAPK
408 activity, within minutes after addition of the chemical inhibitor (Figure 5). This suggests a very
409 direct mechanism of action on the mating pathway. The primary candidate for this process has
410 been Ste5. However, our quantitative measurements speak for an additional mechanism
411 detectable mostly at low pheromone concentrations. Other potential candidate targets of Cdc28
412 could be the G-protein and the receptor, or other proteins in the MAPK signal transduction
413 cascades.

414 The experiments performed with mating mixtures also illustrate that the interplay between the
415 CDK and the MAPK are central elements in the cell fate selected by the cells. Our data indicate
416 that the commitment to the mating program is taking place at low levels of MAPK signaling
417 activity, where we have shown with exogenous pheromone stimulation, that the CDK can
418 frequently override the MAPK arrest. The sensing of the pheromone secreted by nearby mating
419 partners triggers a low level of MAPK activity, including the activation of positive and negative

420 feedback regulation mechanisms (Figure 8). In the cells that will successfully mate, we observe
421 that the MAPK activity is progressively rising and thereby preventing an activation of the CDK
422 that would promote an entry in the cell cycle. The polarized secretion of pheromones by both
423 partners contributes further to this increase in MAPK activity that reaches its maximum shortly
424 before the fusion of the two cells. Cells which are at some distance from a potential partner
425 experience lower levels of pheromone. Internal feedback loops together with the secretion of the
426 Bar1 protease contribute to dampen the MAPK activity thus when cells reach the cell-cycle
427 commitment point the CDK can override this low mating signaling activity and promote a new
428 cell cycle round.

429 Throughout all eukaryotes, MAPK signaling and the cell cycle are highly conserved cellular
430 processes. The homolog of Fus3 in mammalian cells is ERK. ERK is probably best known for its
431 implication in cell growth and division in somatic cells (Meloche and Pouysségur, 2007) and
432 hyperactivating mutation in the ERK pathway are found in numerous cancers (Davies *et al.*,
433 2002). However, the ERK pathway can also inhibit cell cycle progression. One well-known
434 example is the stimulation of PC-12 cells with NGF, which results in a prolonged activation of
435 ERK, promoting a cell cycle arrest and differentiation into neuronal cells (Marshall, 1995;
436 Pumiglia and Decker, 1997). More generally, during development MAPK pathways play a
437 central role in the commitment of cells into specific lineage and this is often performed in tight
438 correlation with the cell cycle (Orford and Scadden, 2008). Correlating dynamic measurements
439 of CDK and MAPK activities in these cells could reveal the underlying mechanisms that allow
440 the MAPK to integrate cell cycle cues to modulate the signaling outcome.

441 Materials and Methods

442 *Strains and plasmids*

443 Yeast strains and plasmids are listed in Supplementary Tables 1 and 2. SKARS plasmids were
444 constructed by cloning the different sensors from Durandau et al (Durandau *et al.*, 2015) into a
445 pSIV vector backbone (Wosika *et al.*, 2016). The sensor and the corrector were assembled by
446 cloning the $STE7_{1\text{-}33}$ *-NLS-NLS-mCherry* or the $STE7_{ND}$*-NLS-NLS-CFP* (HindIII-KpnI)
447 sequences downstream the p*RPS6B* promoter into the pSIV-URA (SacI-KpnI). The plasmid
448 pED141 containing both sensor and corrector was obtained by cloning the p*RPS6B* -$STE7_{ND}$ -

449 *NLS-NLS-CFP* into the second MCS of pED92 (AatII-SphI). Plasmids were transformed in yeast
450 of W303 background expressing the Hta2-iRFP (yED136) or the Hta2-tdiRFP (yED152). Whi5
451 was tagged with mCitrine using pGTT-mCitrine plasmid (Wosika *et al.*, 2016). Kss1 was tagged
452 with mScarlet (pGTL-mScarlet). p*AGA1* induction was monitored by integrating the p*AGA1*-
453 dPSTR^R in the URA3 locus (Aymoz *et al.*, 2018).

454 Genomic deletions were constructed in cells bearing the sensors using KAN or NAT resistance
455 cassettes (Longtine *et al.*, 1998; Goldstein and McCusker, 1999). Plasmids containing the coding
456 sequence of Ste5, Ste20 and Ste7 were obtained by amplification of a chromosome fragment
457 spanning from -100bp (into the promoter) to the end of the ORF and cloned using PacI-NheI
458 sites into the pGTH-CFP (replacing the fluorescent protein). Mutated variants were then obtained
459 by replacing a portion of the plasmid DNA coding sequence by a synthetic double-stranded DNA
460 fragment bearing the desired mutations. Plasmids were integrated into the genome of yeast by
461 replacing the NAT or KAN cassettes used to delete the native gene using homology regions in
462 the promoter of the gene and in the TEF terminator of the deletion cassette, which is also present
463 on the pGTH vector.

464 *Sample preparation*

465 The cells were grown to saturation in overnight cultures at 30°C in synthetic medium (YNB:
466 CYN3801, CSM: DCS0031, ForMedium). They were diluted in the morning to OD_{600}=0.05 and
467 grown for at least four hours before starting the experiments. For experiments in wells, 96-well
468 plates (MGB096-1-2LG, Matrical Bioscience) were coated with a filtered solution of
469 Concanavalin A (0.5 mg/ml, 17-0450-01, GE Healthcare) for 30min, rinsed with H_2O, and dried
470 for at least 2 hours. Before the experiment, the cultures were diluted to an OD_{600} of 0.05, and
471 briefly sonicated. A volume of 200µl of culture was loaded into each well. Cells were left
472 settling 30–45 minutes before imaging. To stimulate the cells, 100µl of inducing solution was
473 added to the wells. For α-factor stimulation, final concentration is indicated into the figure
474 legend. To inhibit the *cdc28-as*, a 25mM stock solution of NAPP1 (A603004, Toronto Research
475 Chemical) in DMSO was diluted in SD-medium and added to the wells. The final working
476 concentration is indicated in the figure legend. For control experiments, cells were treated with
477 DMSO 0.16% in SD-full.

478 For mating assay experiments, log phase cultures of *MAT***a** and *MAT*α (ySP694) were diluted to
479 OD 0.1 in 500µl SD-full. Cells were spun down for 2min at 3000rpm. The supernatant was
480 removed from the cultures and *MAT*α cells were resuspended in 10µl of SD-full. These 10µl
481 were then used to resuspend the *MAT***a** cells. 1µl of this mating mixture was placed on an agar
482 pad. The pad was then placed upside down into the well of a 96-well plate. To prepare the pad, a
483 2% agarose mixture in SD-full was heated for 5 min at 95°. 150µl liquid was placed in a home-
484 made aluminum frame. After cooling down, the 7 mm square pad was gently extracted from the
485 frame. Typically, 6 to 8 mating pads were prepared and imaged in parallel.

486 *Microscopy*

487 Images were acquired with a fully automated inverted epi-fluorescence microscope (Ti-Eclipse,
488 Nikon), controlled by Micromanager software (Edelstein *et al.*, 2010) and placed in an
489 incubation chamber set at 30 °C, with a 40X oil objective and appropriate excitation and
490 emission filters. The excitation was provided by a solid-state light source (SpectraX, Lumencor).
491 The images were recorded with a sCMOS camera (Flash4.0, Hamamatsu). A motorized XY-
492 stage allowed recording multiple fields at every time points. Cy5p5 (200ms), CFP (100ms), RFP
493 (100ms), YFP (300ms) and two brightfield (10ms) images were recorded at time intervals of 3 or
494 5 minutes.

495 *Data analysis*

496 Time-lapse movies were analyzed with the YeastQuant platform (Pelet *et al.*, 2012). The cell
497 nuclei were segmented by thresholding from Cy5p5 images. The contour of the cell around each
498 identified nucleus was detected using both brightfield images. The cytoplasm object was
499 obtained by removing the nucleus object expanded by two pixels from the cell object. The nuclei
500 were tracked across all the frames of the movie. Multiple features of each object were quantified.
501 Note that for mating pad experiments, the *MAT*α cells were not segmented as they do not express
502 the Hta2-iRFP. Dedicated scripts were written in Matlab R2016b (The Mathworks) to further
503 analyze the data. Except for Figure 7, only cells tracked from the beginning to the end of the
504 movie were taken into consideration. In addition, a quality control was applied on each trace and
505 only the traces with low variability in nuclear and cell area, and Cy5p5 nuclear fluorescence

506 were kept for further analysis. On average, 65% of the cells tracked from the beginning to the
507 end of the time lapse passed the quality control.

508 For each cell, the average nuclear intensity in the fluorescent channel corresponding to the
509 SKARS, the Corrector and Whi5-mCitrine were divided by the average intensity in the
510 cytoplasm for every time point (ratio N/C). To quantify the MAPK activity, the Adjusted ratio
511 for each individual cell was obtained by dividing the ratio N/C of the Corrector by the ratio N/C
512 of the SKARS. The CDK activity of each cell was defined as the inverse of the Whi5-mCitrine
513 N/C ratio. The initial CDK activity was defined as the average of three time-points before the
514 stimulus (3–6 minutes before α-factor stimulus). All these quantities are unitless numbers, since
515 they are ratios between fluorescence intensities obtained from the microscope camera. We used
516 the symbol [–] to represent this lack of units.

517 *CDK activity-based clustering and synchronization*

518 When plotting a histogram using the Whi5 ratio N/C (Nuclear intensity over Cytoplamsic
519 intensity) of all cells at all time points, we identified two populations. To properly distinguish
520 between ratios corresponding to nuclear Whi5 versus ratios corresponding to cytoplasmic Whi5,
521 we first separated ratio values using a fixed threshold (threshold=2). However, this value
522 overestimated the limit of what could be considered as nuclear Whi5. We then identified cells
523 with ratios below this threshold at all time points and replotted a histogram of all Whi5 ratio N/C
524 values from this sub-population. This method enables to enrich the sample with low N/C ratio.
525 This second histogram presented a clearer overview of the values corresponding to cytoplasmic
526 Whi5. We then calculated the derivative of the histogram and identified the position of fifth-
527 lowest derivative value. The corresponding Whi5 ratio N/C was used as a final threshold to
528 separate nuclear to cytoplasmic Whi5 values. This procedure enables to correct for slight
529 differences between experiments mostly due to the chosen experimental settings (96 well-plate
530 or pad experiments). Globally, the procedure adjusted the threshold between 2 and 1.7. If the
531 Whi5 ratio N/C was above the threshold, corresponding to a low CDK activity value (C/N) and
532 thus the cell was considered in G1. On the opposite, values below the threshold indicate that the
533 cell was *Out-of-G1*. *G1* cells sub-population was defined by single cell traces which remained
534 above the threshold for the entire duration of the time lapse. Conversely, *Out-of-G1* cells cluster
535 was defined by traces that stay below this threshold. The other single cell traces are scanned for

536 G1-entry and G1-exit events. If a pattern of two values below the threshold followed by two
537 values above the threshold was found, we considered that the cell belonged to the *G1-entry*
538 cluster. The same strategy was used to identify the *G1-exit* sub-population, using a pattern of two
539 values above the threshold followed by two values below the threshold. Cells in the *G1-entry*
540 cluster were defined as having a single event of G1-entry. Cells in the *G1-exit* cluster were
541 selected as having only one event of G1-exit. Finally, the *Through-G1* cluster is made of cells
542 that display a G1-entry event followed by a G1-exit event. Because the duration of the time-lapse
543 experiments is much shorter than the cell cycle of the yeast (45 min vs. 90 min), we considered
544 that the number of events cannot exceed two. Cells which do not follow this criterion were
545 rejected from the analysis. Depending on the experiment, we rejected a maximum of 5% of the
546 total population. The position of the G1-entry was used to create new time vectors for
547 synchronization of the *G1-entry* and the *Through-G1* single cell traces. We extracted the
548 individual time vector for each cell and subtracted the time at which the G1-entry event occurred.

549 *Detection of fusion events in mating assays*

550 *MAT*α cells express the CFP fluorescent protein under the control of a strong promoter. When
551 *MAT***a** and *MAT*α cells fuse the CFP from the *MAT*α cell diffuses into the partner leading to a
552 rise of the fluorescence into the segmented *MAT***a**. Fusing *MAT***a** cells were first detected
553 bioinformatically by identifying a sudden increase of the CFP intensity in the nucleus object. We
554 chose the nucleus object rather than the whole cell to avoid that mis-segmentation triggers a
555 misleading increase in CFP intensity not linked to a fusion event. Fusion event time was defined
556 as the time point at which the difference in the CFP nuclear signal between two consecutive time
557 points exceed 200, while remaining below 700. Traces of fusing cells were selected as they
558 contain a single detected fusion event. We filtered out cells with aberrant absolute and derivative
559 nuclear CFP fluorescence signal or tracked for less than 15 min prior or after the fusion time.
560 CFP images corresponding to selected cells were checked manually to reject false positives that
561 could not be detected during the bioinformatics analysis. The position of the fusion event into the
562 time vectors of individual fusing cells was used as a time reference to align temporally the
563 MAPK activity and CDK (Figure 7).

564 **Acknowledgments**

565 We thank all members of the Pelet and Martin labs for helpful discussions and comments on the
566 manuscripts, Marta Schmitt and Clémence Varidel for technical assistance. This study was
567 supported by Swiss National Science Foundation grants (PP00P3_139121) and the University of
568 Lausanne.

569 Author contributions

570 ED and SP conceived and study and wrote the manuscript. ED constructed the strains and
571 performed the experiments with exogenous stimulation of pheromone. SP performed the mating
572 assay experiments. ED analyzed the single cell data.
573 The authors have declared that no competing interests exist.

574 Figure Legends

575 **Figure 1: Dynamic MAPK and CDK activity measurements in live single cells.**

576 **A.** Schematic representation of the Synthetic Kinase Activity Relocation Sensor (SKARS).

577 **B.** Epi-fluorescence microscopy images of WT cells expressing a Hta2-tdiRFP (nucleus), a
578 $Ste7_{DS}$-SKARS-mCherry (MAPK activity sensor), a $Ste7_{ND}$-SKARS-CFP (Corrector), and a
579 Whi5-mCitrine (CDK activity). Log-phase cells were placed in a microscopy well-plate. During
580 the time lapse, cells were stimulated with 1 μM α-factor (time 0).

581 **C.** MAPK activity was quantified from time-lapse movies acquired with a WT strain (red, Nc =
582 191) and a mating signaling dead mutant (*ste5 Δ*, blue, Nc = 437) (See Methods and
583 Supplementary Figure 1). For all similar graphs, the solid line represents the median of the
584 population, the shaded area delimits the 25 and 75 percentiles of the population. Dashed lines
585 display the response of a few single cells. Nc represents the number of single-cell traces
586 analyzed.

587 **D.** Schematic representation of the CDK activity sensor (Whi5-mCitrine).

588 **E.** Microscopy images of the same strain presented in B. The thumbnails are extracted from a
589 120 min time-lapse movie of unstimulated cells dividing under normal growth conditions.

590 **F**. CDK activity reported as function of time relative to G1. Single cell traces that exhibit at least
591 one trough of CDK activity were selected (Nc = 70). The traces were synchronized relative to the
592 time at which the CDK activity reaches its minimum value (see Supplementary Figure 2).

593

594 **Figure 2: Dynamics of MAPK activity monitored by the SKARS in different cell cycle**
595 **phases.**

596 **A-D.** MAPK activity was quantified for cells in an asynchronously growing culture stimulated
597 with 1 μM α-factor at time 0. 738 single cell traces were clustered by comparing the CDK
598 activity prior and after stimulation (see Methods). *G1* cells (A, Nc =143) retain a low CDK
599 activity throughout the time lapse, while *Out-of-G1* cells (B, Nc =256) maintain a high CDK
600 activity. *G1-exit* cells (C, Nc =76) start with low and finish with high CDK activity. Conversely,
601 *G1-entry* cells (D, Nc =249) start with high and finish with low CDK activity. In this sub-
602 population, the traces are aligned relative to the time of G1-entry. The median (solid line) MAPK
603 activity (red) and CDK activity (green) and the 25–75 percentiles (shaded area) of each sub-
604 population are plotted.

605 **E.** Summary of the various dynamic MAPK activities observed upon addition of 1 μM α-factor
606 at time 0 in the four main cell cycle clusters. Each line corresponds to the mean of the medians of
607 5 biological replicates. Error bars represent the standard deviations of the medians. The
608 percentages in the legend indicate the relative proportion of each cluster in the population.

609 **Figure 3: Commitment to cell cycle is pheromone dose-dependent.**

610 **A-C.** Pheromone dose-dependent dynamic MAPK activity in different phases of the cell cycle.
611 Experiments and clustering analysis were performed as in Figure 2. Different α-factor
612 concentrations were used to stimulate cells. Median MAPK activity from at least five replicates
613 were averaged for each curve. The error bars represent the standard deviations between the
614 replicates.

615 **D.** Fractions of cells in each sub-population as function of the pheromone concentration for our
616 45 min time lapse. The prevalence of each cluster is calculated from the means of at least three
617 replicates.

618

619 **Figure 4: Level of MAPK activity at START controls cell cycle commitment.**

620 **A-C.** Dynamic CDK activity of cells exiting G1 at various pheromone concentrations. Single cell
621 traces (dashed lines) and the median of the sub-population (solid line) are presented in each
622 graph. Note the decreased variability in CDK activity patterns as pheromone concentration
623 increases.

624 **D.** Initial CDK activity (mean of the three points before stimulus) measured in the *G1-exit* cluster
625 for different α-factor concentrations. The distribution of the initial CDK of *G1-exit* cells for one
626 replicate for each concentration is presented as a boxplot. The dots correspond to the median
627 initial CDK activity of additional replicates.

628 **E.** CDK activity of cells attempting to exit G1. The dynamic CDK activity of G1 cells from
629 multiple 1000nM α-factor experiments were pooled. The Attempt G1-exit sub-population (red)
630 contains cells with an initial CDK activity above 0.35. Four single cell traces from the Attempt
631 G1-exit sub-population (dashed lines) that display a transient peak in CDK activity around the
632 time of pheromone addition are plotted. The median CDK activity for the *G1* (blue) and *G1-exit*
633 (green) clusters from Figure 2 are plotted for comparison.

634

635 **Figure 5: Regulation of MAPK signal transduction by the CDK.**

636 **A-B.** Dynamic CDK and MAPK activities after *cdc28-as* chemical inhibition. Cells expressing
637 an analog sensitive allele of Cdc28 (*cdc28-as*) are imaged every two minutes for 50 minutes.
638 Cells are stimulated with 100nM α-factor at time 0. Six minutes later either NAPP1 (10 μM,
639 solid line and shaded area) or DMSO (0.04% v/v, dashed line) is added. MAPK and CDK
640 activities of cells starting *Out-of-G1* (mean $CDK_{t<0}$ >0.5, A, NAPP1: Nc = 448, DMSO: Nc =
641 381), or exiting G1 upon pheromone addition (mean $CDK_{t<0}$ <0.5 and mean $CDK_{0<t<6}$ >0.5, B,
642 NAPPI: Nc = 39, DMSO: Nc = 16) are plotted.

643 **Figure 6: Dynamic MAPK activity of cells expressing non-phosphorylatable Ste5 alleles.**

644 **A.** Schematic representation of the wild-type Ste5 scaffold protein structure compared to the
645 $Ste5_{8A}$ mutant with 8 non-phosphorylatable residues in the vicinity of the plasma membrane
646 domain and the $Ste5_{CND}$ variant with point mutations in the Cln1/2 docking motif.

647 **B-D.** Dynamics of mating pathway activity in *G1* (solid line) and *G1-exit* cells (dashed line)
648 measured by the SKARS (B), Kss1 relocation (cytoplasmic over nuclear intensity, C) and
649 p*AGA1*-dPSTR^{R} nuclear accumulation (nucleus minus cytoplasmic intensity, D). Cells
650 expressing either the $Ste5_{WT}$ (blue), $Ste5_{8A}$ (red), or $Ste5_{CND}$ allele (yellow) were treated with
651 10nM (left) and 100nM (right) pheromone. Cell cycle clustering was performed as in Figure 2.
652 Median MAPK activity from at least three replicates were averaged for each curve. The error
653 bars represent the standard deviations between the replicates.

654 **Figure 7: CDK and MAPK cross-regulation in mating conditions**

655 **A.** Microscopy time-lapse images of two fusion events between *MAT***a** cells expressing the
656 various sensors mixed with *MAT*α strain expressing a cytoplasmic CFP. The fusion can be
657 detected when the CFP from the *MAT*α diffuses in the *MAT***a** partner (White arrows). The
658 indicated time is relative to the last time point preceding the second fusion event.

659 **B.** Dynamic MAPK and CDK activities in *MAT***a** cells undergoing fusion detected by a sharp
660 increase in CFP intensity (blue) (See Method). MAPK (red) and CDK (green) activities of the
661 fusing cells were synchronized relative to the last time point before the fusion occurs (Nc=127).
662 The dashed orange line and the shaded area around it correspond to the median and 25–75
663 percentiles (averaged across multiple time points) of the MAPK activity in *MAT***a** cells in
664 absence of mating partners, but imaged in the same conditions.

665 **C-D.** Duration of the G1 phase of non-fusing cells. Non-fusing cells transiting through G1 were
666 identified as previously (Figure 3C and Methods). **C.** The time separating the G1 entry and G1
667 exit is calculated from each single cell trace ($\Delta t_{exit-entry}$) and averaged. The means $\Delta t_{exit-entry}$
668 from at least three replicates are plotted as boxplot. **D.** The dynamic CDK activity from single
669 cells are synchronized relative to the G1 entry. Error bars are standard deviation of at least three
670 medians replicates.

671 **E.** MAPK activity in non-fusing *MAT***a** cells transiting through G1. Single cell traces are
672 synchronized relative to the G1 entry and averaged as in Figure 2D. Error bars are standard
673 deviation of at least three medians replicates.

674 In these mating experiments, all strains are BAR1.

675 **Figure 8: Scheme of the interplay between CDK and MAPK during mating**

676 *MAT***a** cells respond to a pheromone gradient secreted by a *MAT*α mating partner. The strength
677 of the MAPK activity will depend on the level of α-factor sensed by the cells and the
678 contribution of positive and negative feedback. At START, relative CDK and MAPK activities
679 will be compared in order for the cell to select a fate: division or mating.

680 # References

681 Atay, O., and Skotheim, J. M. (2017). Spatial and temporal signal processing and decision making by MAPK
682 pathways. J Cell Biol *216*, 317–330.

683 Aymoz, D., Solé, C., Pierre, J.-J., Schmitt, M., de Nadal, E., Posas, F., and Pelet, S. (2018). Timing of gene
684 expression in a cell-fate decision system. Molecular Systems Biology *14*, e8024.

685 Aymoz, D., Wosika, V., Durandau, E., and Pelet, S. (2016). Real-time quantification of protein expression at the
686 single-cell level via dynamic protein synthesis translocation reporters. Nature Communications *7*, 11304.

687 Bardwell, L. (2005). A walk-through of the yeast mating pheromone response pathway. Peptides *26*, 339–350.

688 Bean, J. M., Siggia, E. D., and Cross, F. R. (2006). Coherence and timing of cell cycle start examined at single-cell
689 resolution. Mol Cell *21*, 3–14.

690 Bhaduri, S., and Pryciak, P. M. (2011). Cyclin-specific docking motifs promote phosphorylation of yeast signaling
691 proteins by G1/S Cdk complexes. Curr Biol *21*, 1615–1623.

692 Bhattacharyya, R. P., Reményi, A., Good, M. C., Bashor, C. J., Falick, A. M., and Lim, W. A. (2006). The Ste5
693 scaffold allosterically modulates signaling output of the yeast mating pathway. Science *311*, 822–826.

694 Bishop, A. C. *et al.* (2000). A chemical switch for inhibitor-sensitive alleles of any protein kinase. Nature *407*, 395–
695 401.

696 Chang, F., and Herskowitz, I. (1990). Identification of a gene necessary for cell cycle arrest by a negative growth
697 factor of yeast: FAR1 is an inhibitor of a G1 cyclin, CLN2. Cell *63*, 999–1011.

698 Charvin, G., Cross, F. R., and Siggia, E. D. (2008). A microfluidic device for temporally controlled gene expression
699 and long-term fluorescent imaging in unperturbed dividing yeast cells. PLoS ONE *3*, e1468.

700 Chen, R. E., and Thorner, J. (2007). Function and regulation in MAPK signaling pathways: lessons learned from the
701 yeast Saccharomyces cerevisiae. Biochim Biophys Acta *1773*, 1311–1340.

702 Cherkasova, V., Lyons, D. M., and Elion, E. A. (1999). Fus3p and Kss1p control G1 arrest in Saccharomyces
703 cerevisiae through a balance of distinct arrest and proliferative functions that operate in parallel with Far1p.
704 Genetics *151*, 989–1004.

705 Clement, S. T., Dixit, G., and Dohlman, H. G. (2013). Regulation of yeast G protein signaling by the kinases that
706 activate the AMPK homolog Snf1. Science Signaling *6*, ra78.

707 Clotet, J., and Posas, F. (2007). Control of cell cycle in response to osmostress: lessons from yeast. Meth
708 Enzymol *428*, 63–76.

709 Conlon, P., Gelin-Licht, R., Ganesan, A., Zhang, J., and Levchenko, A. (2016). Single-cell dynamics and variability
710 of MAPK activity in a yeast differentiation pathway. Proc Natl Acad Sci USA *113*, E5896–E5905.

711 Costanzo, M., Nishikawa, J. L., Tang, X., Millman, J. S., Schub, O., Breitkreuz, K., Dewar, D., Rupes, I., Andrews,
712 B., and Tyers, M. (2004). CDK activity antagonizes Whi5, an inhibitor of G1/S transcription in yeast. Cell *117*,
713 899–913.

714 Davies, H. *et al.* (2002). Mutations of the BRAF gene in human cancer. Nature *417*, 949–954.

715 de Bruin, R. A. M., McDonald, W. H., Kalashnikova, T. I., Yates, J., and Wittenberg, C. (2004). Cln3 activates G1-
716 specific transcription via phosphorylation of the SBF bound repressor Whi5. Cell *117*, 887–898.

717 Dirick, L., Böhm, T., and Nasmyth, K. (1995). Roles and regulation of Cln-Cdc28 kinases at the start of the cell
718 cycle of Saccharomyces cerevisiae. Embo J *14*, 4803–4813.

719 Doncic, A., Atay, O., Valk, E., Grande, A., Bush, A., Vasen, G., Colman-Lerner, A., Loog, M., and Skotheim, J. M.
720 (2015). Compartmentalization of a bistable switch enables memory to cross a feedback-driven transition. Cell *160*,
721 1182–1195.

722 Doncic, A., Falleur-Fettig, M., and Skotheim, J. M. (2011). Distinct interactions select and maintain a specific cell
723 fate. Mol Cell *43*, 528–539.

724 Durandau, E., Aymoz, D., and Pelet, S. (2015). Dynamic single cell measurements of kinase activity by synthetic
725 kinase activity relocation sensors. BMC Biol. *13*, 55.

726 Edelstein, A., Amodaj, N., Hoover, K., Vale, R., and Stuurman, N. (2010). Computer control of microscopes using
727 µManager. Curr Protoc Mol Biol *Chapter 14*, Unit14.20.

728 Escoté, X., Zapater, M., Clotet, J., and Posas, F. (2004). Hog1 mediates cell-cycle arrest in G1 phase by the dual
729 targeting of Sic1. *6*, 997–1002.

730 Goldstein, A. L., and McCusker, J. H. (1999). Three new dominant drug resistance cassettes for gene disruption in
731 Saccharomyces cerevisiae. Yeast *15*, 1541–1553.

732 Hao, N., Yildirim, N., Wang, Y., Elston, T. C., and Dohlman, H. G. (2003). Regulators of G protein signaling and
733 transient activation of signaling: experimental and computational analysis reveals negative and positive feedback
734 controls on G protein activity. J Biol Chem *278*, 46506–46515.

735 Hartwell, L. H., Culotti, J., Pringle, J. R., and Reid, B. J. (1974). Genetic control of the cell division cycle in yeast.
736 Science *183*, 46–51.

737 Longtine, M. S., McKenzie, A., Demarini, D. J., Shah, N. G., Wach, A., Brachat, A., Philippsen, P., and Pringle, J.
738 R. (1998). Additional modules for versatile and economical PCR-based gene deletion and modification in
739 Saccharomyces cerevisiae. Yeast *14*, 953–961.

740 Marshall, C. J. (1995). Specificity of Receptor Tyrosine Kinase Signaling - Transient Versus Sustained Extracellular
741 Signal-Regulated Kinase Activation. Cell *80*, 179–185.

742 McKinney, J. D., Chang, F., Heintz, N., and Cross, F. R. (1993). Negative regulation of FAR1 at the Start of the
743 yeast cell cycle. Genes & Development *7*, 833–843.

744 Meloche, S., and Pouysségur, J. (2007). The ERK1/2 mitogen-activated protein kinase pathway as a master regulator
745 of the G1- to S-phase transition. Oncogene *26*, 3227–3239.

746 Mohl, D. A., Huddleston, M. J., Collingwood, T. S., Annan, R. S., and Deshaies, R. J. (2009). Dbf2-Mob1 drives
747 relocalization of protein phosphatase Cdc14 to the cytoplasm during exit from mitosis. J Cell Biol *184*, 527–539.

748 Nagiec, M. J., and Dohlman, H. G. (2012). Checkpoints in a yeast differentiation pathway coordinate signaling
749 during hyperosmotic stress. PLoS Genetics *8*, e1002437.

750 Nagiec, M. J., McCarter, P. C., Kelley, J. B., Dixit, G., Elston, T. C., and Dohlman, H. G. (2015). Signal inhibition
751 by a dynamically regulated pool of monophosphorylated MAPK. Mol Biol Cell *26*, 3359–3371.

752 Oda, Y., Huang, K., Cross, F. R., Cowburn, D., and Chait, B. T. (1999). Accurate quantitation of protein expression
753 and site-specific phosphorylation. Proc Natl Acad Sci USA *96*, 6591–6596.

754 Oehlen, L. J., and Cross, F. R. (1994). G1 cyclins CLN1 and CLN2 repress the mating factor response pathway at
755 Start in the yeast cell cycle. Genes & Development *8*, 1058–1070.

756 Oehlen, L. J., and Cross, F. R. (1998). Potential regulation of Ste20 function by the Cln1-Cdc28 and Cln2-Cdc28
757 cyclin-dependent protein kinases. J Biol Chem *273*, 25089–25097.

758 Oehlen, L. J., Jeoung, D. I., and Cross, F. R. (1998). Cyclin-specific START events and the G1-phase specificity of
759 arrest by mating factor in budding yeast. Mol. Gen. Genet. *258*, 183–198.

760 Oehlen, L. J., McKinney, J. D., and Cross, F. R. (1996). Ste12 and Mcm1 regulate cell cycle-dependent transcription
761 of FAR1. Mol Cell Biol *16*, 2830–2837.

762 Orford, K. W., and Scadden, D. T. (2008). Deconstructing stem cell self-renewal: genetic insights into cell-cycle
763 regulation. Nat Rev Genet *9*, 115–128.

764 Pelet, S. (2017). Nuclear relocation of Kss1 contributes to the specificity of the mating response. Sci. Rep. *7*, 43636.

765 Pelet, S., Dechant, R., Lee, S. S., van Drogen, F., and Peter, M. (2012). An integrated image analysis platform to
766 quantify signal transduction in single cells. Integrative Biology : Quantitative Biosciences From Nano to Macro *4*,
767 1274–1282.

768 Peter, M., and Herskowitz, I. (1994). Direct inhibition of the yeast cyclin-dependent kinase Cdc28-Cln by Far1.
769 Science *265*, 1228–1231.

770 Peter, M., Gartner, A., Horecka, J., Ammerer, G., and Herskowitz, I. (1993). FAR1 links the signal transduction
771 pathway to the cell cycle machinery in yeast. Cell *73*, 747–760.

772 Pumiglia, K. M., and Decker, S. J. (1997). Cell cycle arrest mediated by the MEK/mitogen-activated protein kinase
773 pathway. Proc Natl Acad Sci USA *94*, 448–452.

774 Reményi, A., Good, M. C., Bhattacharyya, R. P., and Lim, W. A. (2005). The role of docking interactions in
775 mediating signaling input, output, and discrimination in the yeast MAPK network. Mol Cell *20*, 951–962.

776 Repetto, M. V., Winters, M. J., Bush, A., Reiter, W., Hollenstein, D. M., Ammerer, G., Pryciak, P. M., and Colman-
777 Lerner, A. (2018). CDK and MAPK Synergistically Regulate Signaling Dynamics via a Shared Multi-site
778 Phosphorylation Region on the Scaffold Protein Ste5. Mol Cell *69*, 938–952.e6.

779 Roux, P. P., and Blenis, J. (2004). ERK and p38 MAPK-Activated Protein Kinases: a Family of Protein Kinases
780 with Diverse Biological Functions. Microbiology and Molecular Biology Reviews *68*, 320–344.

781 Roy, A., Lu, C. F., Marykwas, D. L., Lipke, P. N., and Kurjan, J. (1991). The Aga1 Product Is Involved in Cell-
782 Surface Attachment of the Saccharomyces-Cerevisiae Cell-Adhesion Glycoprotein a-Agglutinin. Mol Cell Biol *11*,
783 4196–4206.

784 Saito, H. (2010). Regulation of cross-talk in yeast MAPK signaling pathways. Current Opinion in Microbiology *13*,
785 677–683.

786 Sharifian, H. *et al.* (2015). Parallel feedback loops control the basal activity of the HOG MAPK signaling cascade.

787 Integrative Biology : Quantitative Biosciences From Nano to Macro *7*, 412–422.

788 Shou, W. Y., Seol, J. H., Shevchenko, A., Baskerville, C., Moazed, D., Chen, Z., Jang, J., Charbonneau, H., and
789 Deshaies, R. J. (1999). Exit from mitosis is triggered by Tem1-dependent release of the protein phosphatase Cdc14
790 from nucleolar RENT complex. Cell *97*, 233–244.

791 Strickfaden, S. C., Winters, M. J., Ben-Ari, G., Lamson, R. E., Tyers, M., and Pryciak, P. M. (2007). A mechanism
792 for cell-cycle regulation of MAP kinase signaling in a yeast differentiation pathway. Cell *128*, 519–531.

793 Tyers, M. (1996). The cyclin-dependent kinase inhibitor p40SIC1 imposes the requirement for Cln G1 cyclin
794 function at Start. Proc Natl Acad Sci USA *93*, 7772–7776.

795 Tyers, M., and Futcher, B. (1993). Far1 and Fus3 link the mating pheromone signal transduction pathway to three
796 G1-phase Cdc28 kinase complexes. Mol Cell Biol *13*, 5659–5669.

797 Visintin, R., Hwang, E. S., and Amon, A. (1999). Cfi1 prevents premature exit from mitosis by anchoring Cdc14
798 phosphatase in the nucleolus. Nature *398*, 818–823.

799 Wassmann, K., and Ammerer, G. (1997). Overexpression of the G1-cyclin gene CLN2 represses the mating pathway
800 in Saccharomyces cerevisiae at the level of the MEKK Ste11. J Biol Chem *272*, 13180–13188.

801 Wosika, V., Durandau, E., Varidel, C., Aymoz, D., Schmitt, M., and Pelet, S. (2016). New families of single
802 integration vectors and gene tagging plasmids for genetic manipulations in budding yeast. Molecular Genetics and
803 Genomics *291*, 2231–2240.

804 Wu, C., Leeuw, T., Leberer, E., Thomas, D. Y., and Whiteway, M. (1998). Cell cycle- and Cln2p-Cdc28p-
805 dependent phosphorylation of the yeast Ste20p protein kinase. J Biol Chem *273*, 28107–28115.

806 Yu, R. C., Pesce, C. G., Colman-Lerner, A., Lok, L., Pincus, D., Serra, E., Holl, M., Benjamin, K., Gordon, A., and
807 Brent, R. (2008). Negative feedback that improves information transmission in yeast signaling. Nature *456*, 755–
808 761.

809

810 **Supplementary Material:**

811

812 Supporting Information Legends

813 Supplementary Figures 1 to 11
814 Supplementary Tables 1 and 2

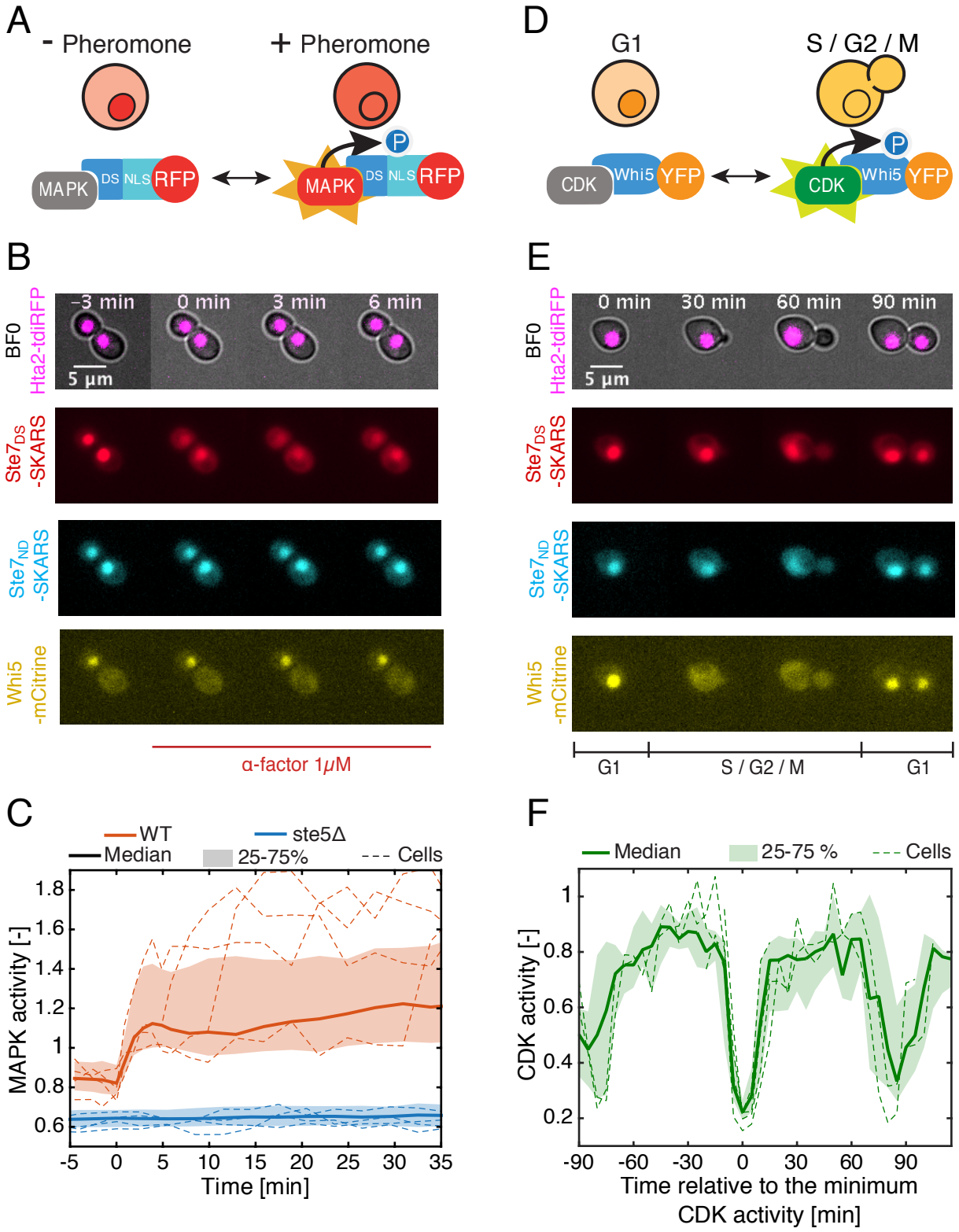
A
- Pheromone
+ Pheromone
MAPK
DS
NLS
RFP
P
B
BF0
Hta2-tdiRFP
-3 min
0 min
3 min
6 min
5 µm
Ste7DS -SKARS
Ste7ND -SKARS
Whi5 -mCitrine
α-factor 1µM
C
WT
ste5Δ
Median
25-75%
Cells
MAPK activity [-]
Time [min]
D
G1
S / G2 / M
CDK
Whi5
YFP
E
30 min
60 min
90 min
G1
S / G2 / M
F
CDK activity [-]
Time relative to the minimum CDK activity [min]

Figure 1

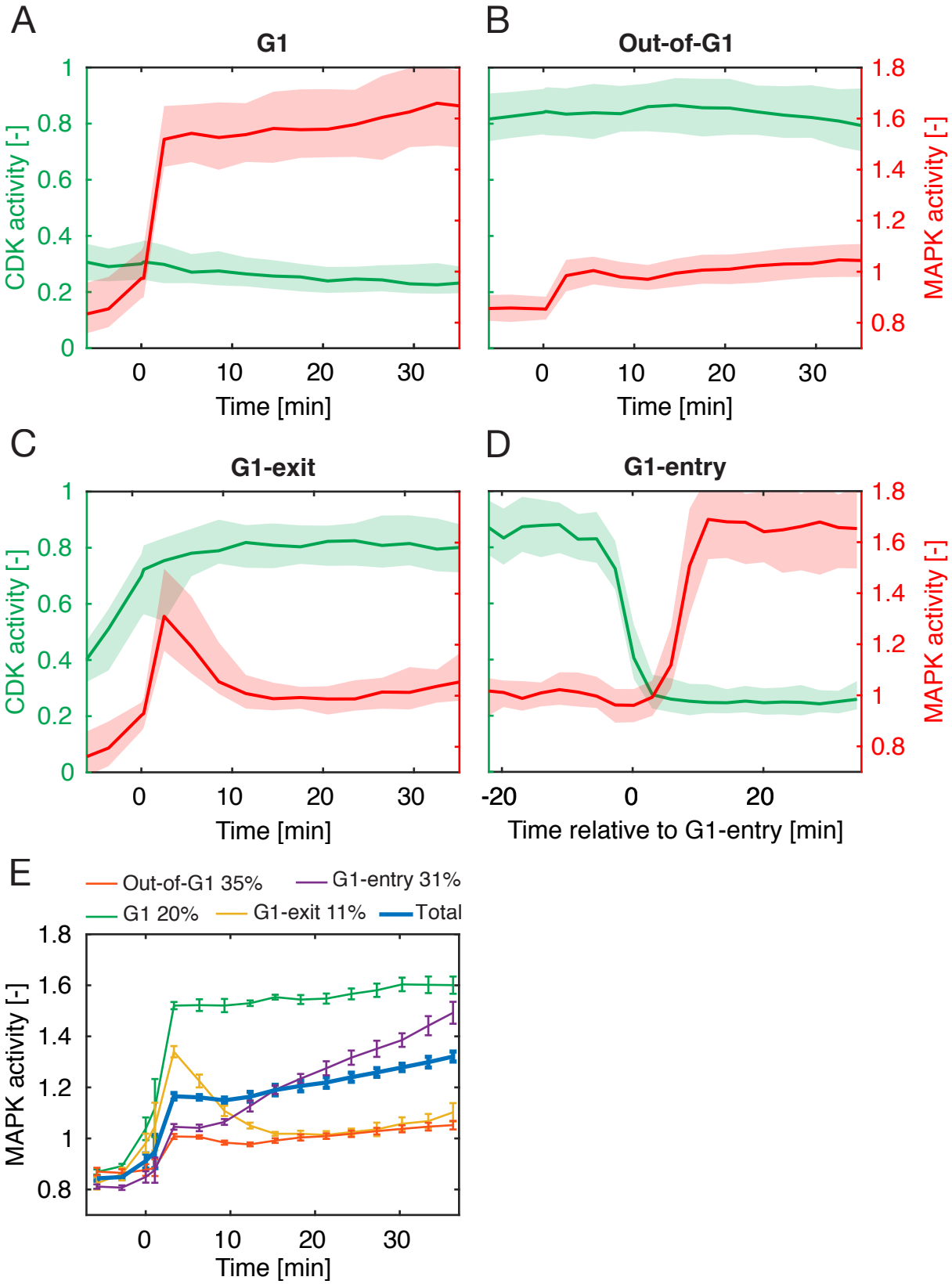
A
G1
B
Out-of-G1
C
G1-exit
D
G1-entry
CDK activity [-]
MAPK activity [-]
Time [min]
Time relative to G1-entry [min]
E
Out-of-G1 35%
G1-entry 31%
G1 20%
G1-exit 11%
Total
MAPK activity [-]
Time [min]

Figure 2

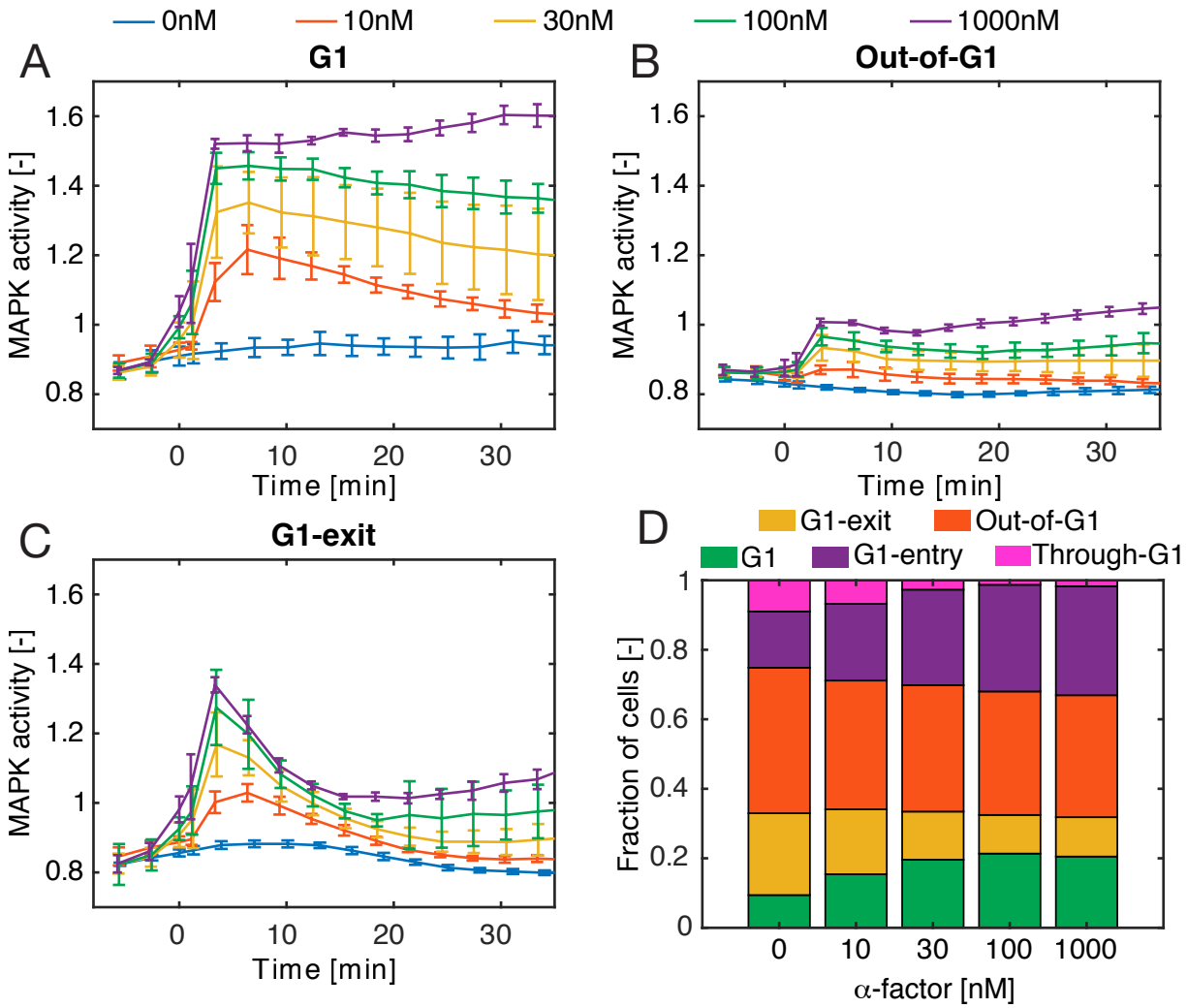
0nM
10nM
30nM
100nM
1000nM
A
G1
B
Out-of-G1
C
G1-exit
D
MAPK activity [-]
Time [min]
Fraction of cells [-]
α-factor [nM]
G1-exit
Out-of-G1
G1
G1-entry
Through-G1

Figure 3

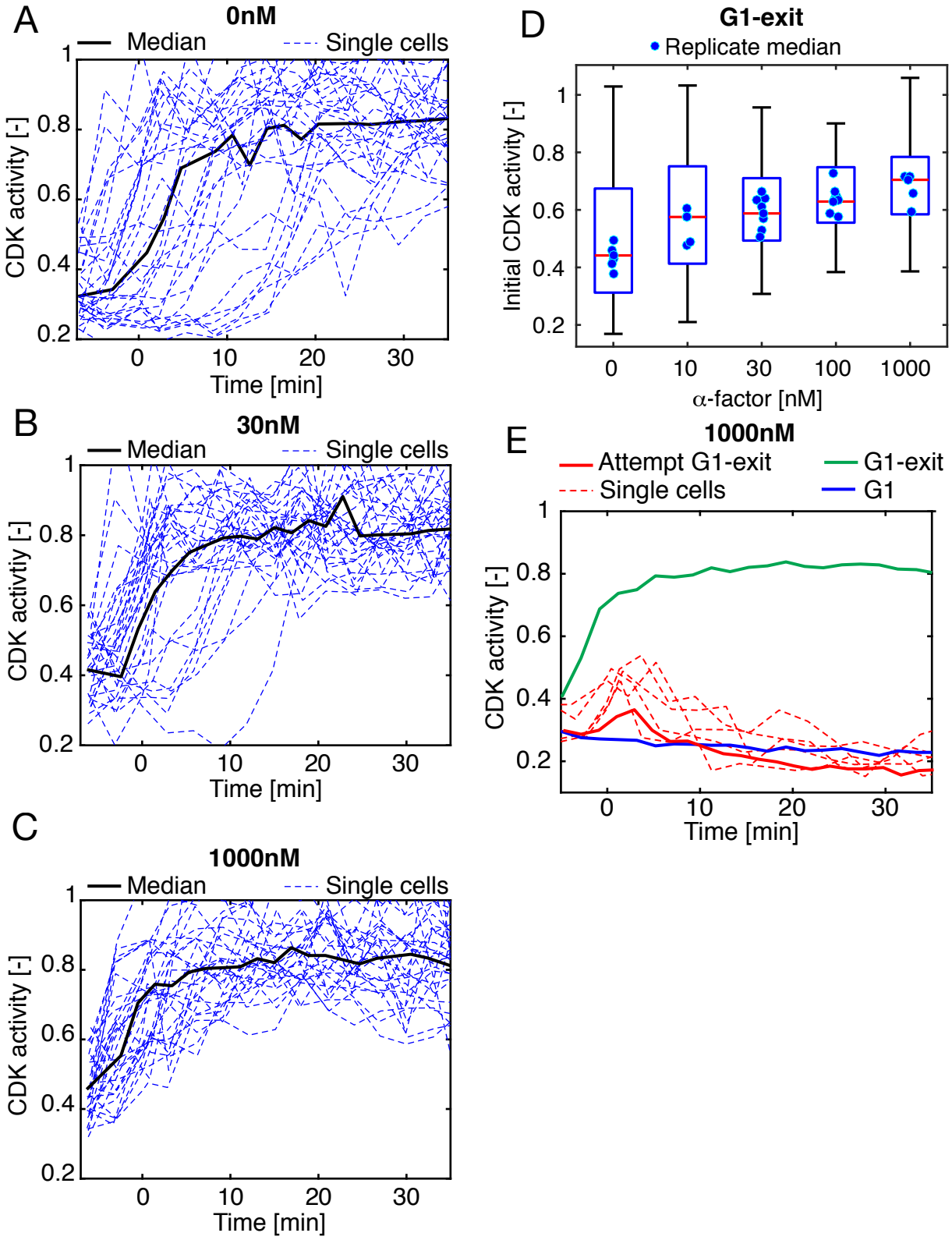
A
0nM
Median
Single cells
CDK activity [-]
Time [min]
B
30nM
Median
Single cells
CDK activity [-]
Time [min]
C
1000nM
Median
Single cells
CDK activity [-]
Time [min]
D
G1-exit
Replicate median
Initial CDK activity [-]
α-factor [nM]
E
1000nM
Attempt G1-exit
Single cells
G1-exit
G1
CDK activity [-]
Time [min]

Figure 4

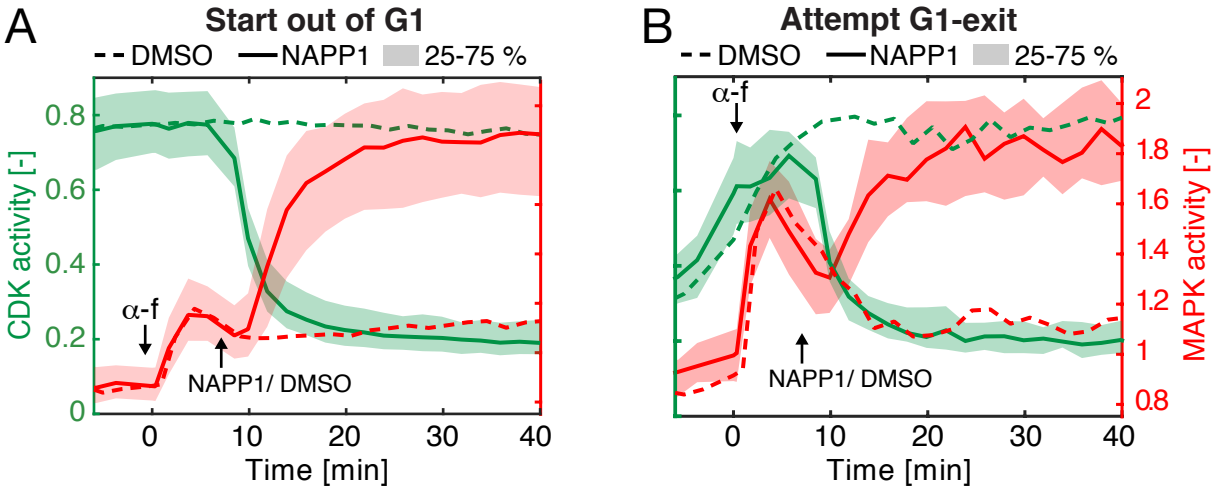
A
Start out of G1
DMSO
NAPP1
25-75 %
CDK activity [-]
0.8
0.6
0.4
0.2
0
α-f
NAPP1/ DMSO
0
10
20
30
40
Time [min]
B
Attempt G1-exit
DMSO
NAPP1
25-75 %
α-f
NAPP1/ DMSO
2
1.8
1.6
1.4
1.2
1
0.8
MAPK activity [-]
0
10
20
30
40
Time [min]

Figure 5

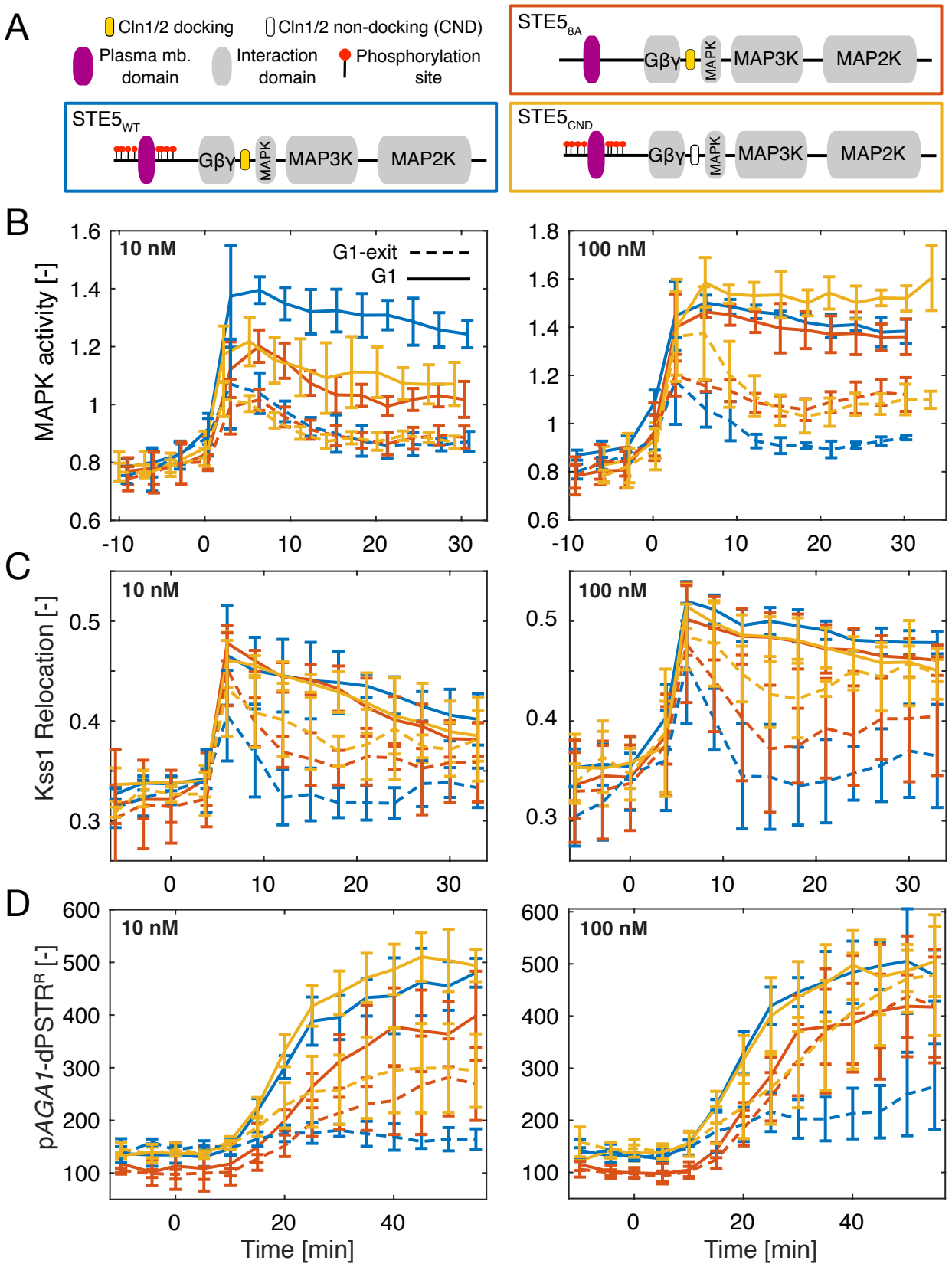
A
Cln1/2 docking
Cln1/2 non-docking (CND)
Plasma mb. domain
Interaction domain
Phosphorylation site
STE5$_{8A}$
STE5$_{WT}$
STE5$_{CND}$
Gβγ
MAPK
MAP3K
MAP2K
B
MAPK activity [-]
10 nM
100 nM
G1-exit
G1
C
Kss1 Relocation [-]
D
pAGA1-dPSTR^R [-]
Time [min]

Figure 6

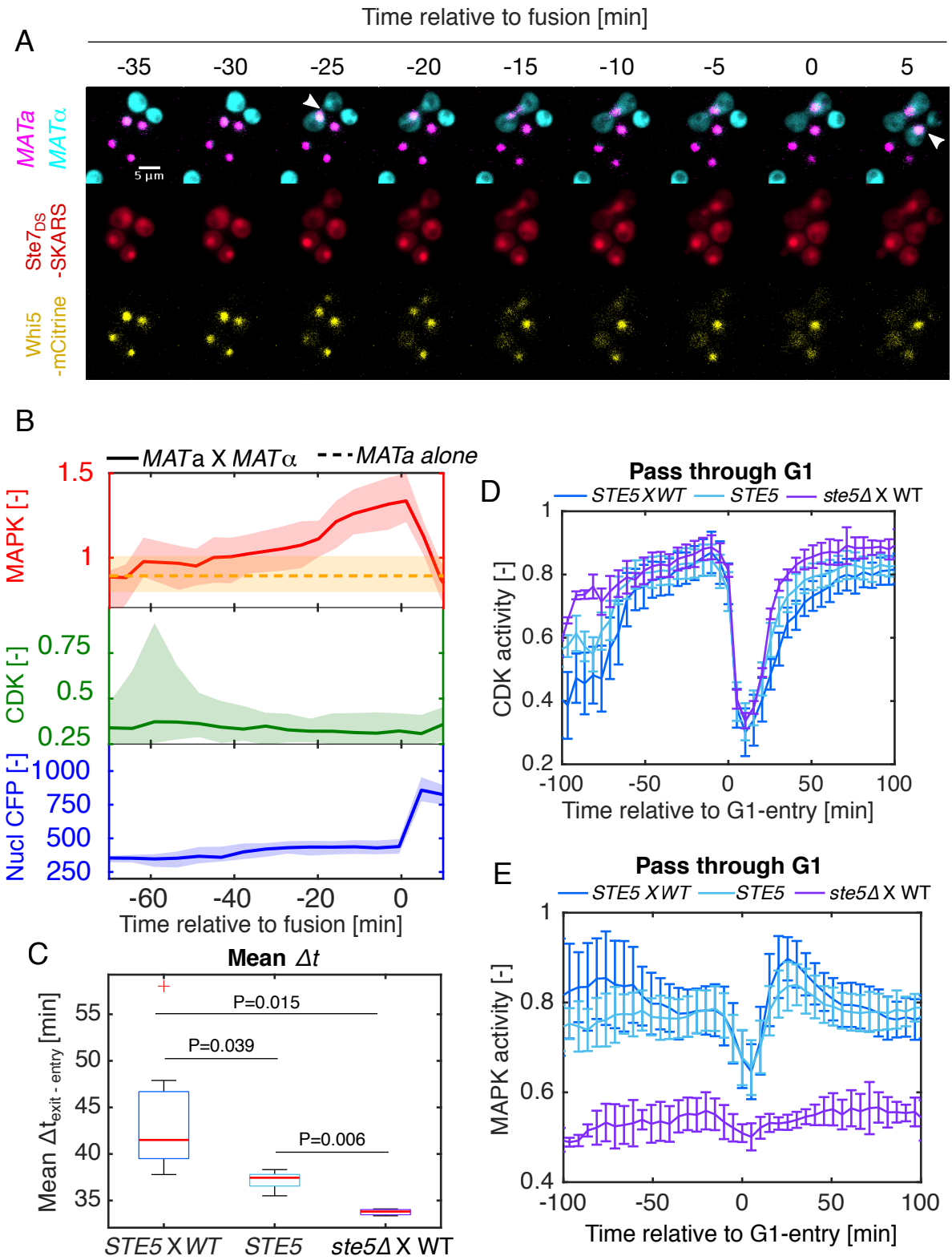
A
Time relative to fusion [min]
-35
-30
-25
-20
-15
-10
-5
0
5
MATa
MATα
5 µm
Ste7DS -SKARS
Whi5 -mCitrine
B
MATa X MATα
MATa alone
MAPK [-]
1.5
1
CDK [-]
0.75
0.5
0.25
Nucl CFP [-]
1000
750
500
250
-60
-40
-20
0
Time relative to fusion [min]
C
Mean Δt
Mean Δtexit - entry [min]
55
50
45
40
35
P=0.015
P=0.039
P=0.006
STE5 X WT
STE5
ste5Δ X WT
D
Pass through G1
STE5 X WT
STE5
ste5Δ X WT
CDK activity [-]
1
0.8
0.6
0.4
0.2
-100
-50
0
50
100
Time relative to G1-entry [min]
E
Pass through G1
STE5 X WT
STE5
ste5Δ X WT
MAPK activity [-]
1
0.8
0.6
0.4
-100
-50
0
50
100
Time relative to G1-entry [min]

Figure 7

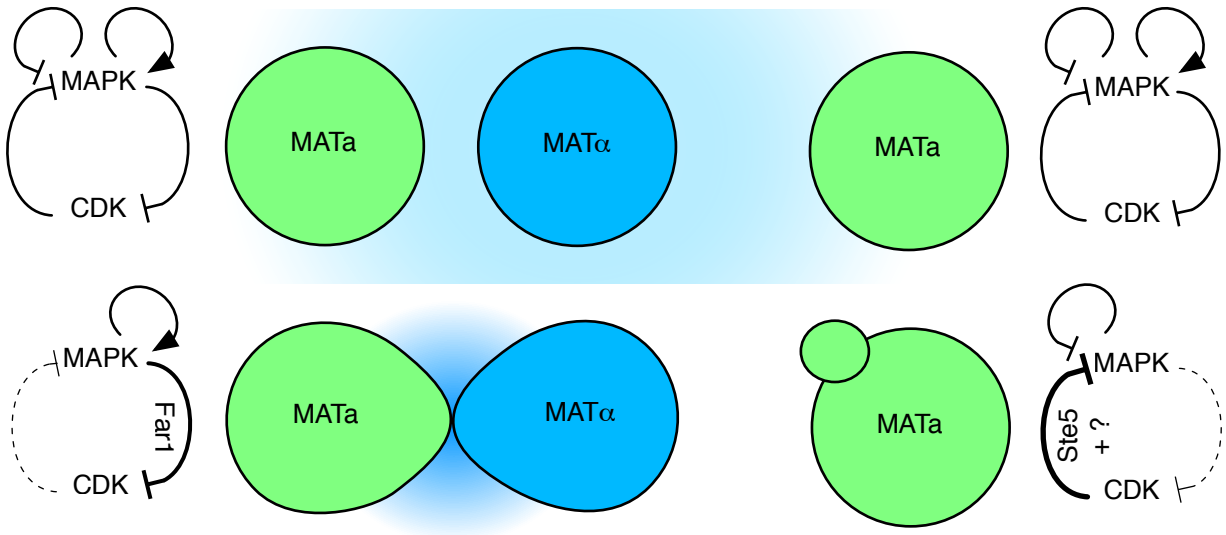
MAPK
CDK
MATa
MATα
MATa
MAPK
CDK
MAPK
Far1
CDK
MATa
MATα
MATa
MAPK
Ste5
+ ?
CDK

Figure 8